Published in final edited form as:
Int J Cardiol. 2014 February 15; 171(3): 431–442. doi:10.1016/j.ijcard.2013.12.084.

ABCC9 is a Novel Brugada and Early Repolarization Syndrome Susceptibility Gene

Dan Hu[a,1,*], **Hector Barajas-Martínez**[a,1], **Andre Terzic**[b], **Sungjo Park**[b], **Ryan Pfeiffer**[a], **Elena Burashnikov**[a], **Yuesheng Wu**[a], **Martin Borggrefe**[c], **Christian Veltmann**[c], **Rainer Schimpf**[c], **John J. Cai**[d], **Gi-Byong Nam**[e], **Pramod Deshmukh**[f], **Melvin Scheinman**[g], **Mark Preminger**[h], **Jonathan Steinberg**[i], **Angélica López-Izquierdo**[j], **Daniela Ponce-Balbuena**[j], **Christian Wolpert**[c], **Michel Haïssaguerre**[k], **José Antonio Sánchez-Chapula**[j], and **Charles Antzelevitch**[a,*]

[a]Department of Molecular Genetics and Experimental Cardiology, Masonic Medical Research Laboratory, Utica, NY, USA

[b]Division of Cardiovascular Diseases, Departments of Medicine, Mayo Clinic, Rochester, MN, USA

[c]1st Department of Medicine-Cardiology, University Medical Centre Mannheim, Mannheim, Germany

[d]Slocum Dickson Medical Group, Utica, NY, USA

[e]Department of Internal Medicine, Asan Medical Center, University of Ulsan College of Medicine, Seoul, Korea

[f]Guthrie Clinic, Sayre, PA, USA

[g]Department of Medicine, University of California, San Francisco, CA, USA

[h]United Medical Practice Association, Ridgewood, NJ, USA

[i]Arrhythmia Institute, Valley Health System, Columbia University College of Physicians & Surgeons, New York, NY, USA

[j]Unidad de Investigación, “Carlos Méndez” del Centro Universitario de Investigaciones Biomédicas de la Universidad de Colima, Colima, México

[k]Hôspital Cardiologique du Haut Lévêque, Université Bordeaux II, Pessac cedex, France

Abstract

Background—Genetic defects in KCNJ8, encoding the Kir6.1 subunit of the ATP-sensitive K^+ channel ($I_{K\text{-}ATP}$), have previously been associated with early repolarization (ERS) and Brugada (BrS) syndromes. Here we test the hypothesis genetic variants in *ABCC9*, encoding the ATP-binding cassette transporter of $I_{K\text{-}ATP}$ (SUR2A), are also associated with both BrS and ERS.

[*]Corresponding authors: C. Antzelevitch (ca@mmrl.edu) and D. Hu (dianah@mmrl.edu). Masonic Medical Research Laboratory, 2150 Bleecker Street, Utica, NY, 13501-1787, USA. Tel.: +1 315 735 2217; fax: +1 315 735 5648.
[1]Authors contributed equally.

Conflict of Interests: none.

Methods and Results—Direct sequencing of all ERS/BrS susceptibility genes was performed on 150 probands and family members. Whole-cell and inside-out patch-clamp methods were used to characterize mutant channels expressed in TSA201-cells. Eight *ABCC9* mutations were uncovered in 11 male BrS probands. Four probands, diagnosed with ERS, carried a highly-conserved mutation, V734I-*ABCC9*. Functional expression of the V734I variant yielded a Mg-ATP IC_{50} that was 5-fold that of wild-type (WT). An 18-y/o male with global ERS, inherited an *SCN5A*-E1784K mutation from his mother, who displayed long QT intervals, and S1402C-*ABCC9* mutation from his father, who displayed an ER pattern. *ABCC9*-S1402C likewise caused a gain of function of $I_{K\text{-}ATP}$ with a shift of ATP IC_{50} from 8.5±2 mM to 13.4±5 μM ($p<0.05$). The *SCN5A* mutation reduced peak I_{Na} to 39% of WT ($p<0.01$), shifted steady-state inactivation by −18.0mV ($p<0.01$) and increased late I_{Na} from 0.14% to 2.01% of peak I_{Na} ($p<0.01$).

Conclusion—Our study is the first to identify *ABCC9* as a susceptibility gene for ERS and BrS. Our findings also suggest that a gain-of-function in $I_{K\text{-}ATP}$ when coupled with a loss-of-function in S*CN5A* may underlie type 3 ERS, which is associated with a severe arrhythmic phenotype.

Keywords

Mutation; ATP-Sensitive Potassium Channel; Sodium Channel; Sudden Cardiac Death; J Wave Syndromes

1. Introduction

Prominent J waves and ST-segment elevation occurring in individuals exhibiting life-threatening arrhythmias without structural heart disease characterize the early repolarization (ERS) and Brugada (BrS) syndromes. Patients with ERS exhibit a characteristic electrocardiogram (ECG) pattern consisting of a J point elevation or distinct J waves, slurring of the terminal part of the QRS and/or ST-segment elevation, most commonly seen in inferior and/or lateral leads. Patients with BrS typically manifest prominent J waves, often referred to as ST segment elevation, in the right precordial leads. Although BrS and ERS differ with respect to the magnitude and lead location of abnormal J wave manifestation, they are thought to represent a continuous spectrum of phenotypic expression termed J wave syndromes[1].

An early repolarization (ER) pattern in the ECG is generally found in healthy young males and has traditionally been viewed as benign[2]. The observation in 2000 that an ER pattern in the canine coronary-perfused wedge preparation can easily convert to one in which phase 2 reentry gives rise to polymorphic ventricular tachycardia/ventricular fibrillation (VT/VF), prompted the suggestion that ER may in some cases predispose to malignant arrhythmias in man[1]. A definitive association between ER and idiopathic VF was presented in the form of two studies published in the *New England Journal of Medicine* in 2008 [3,4]. These were followed by another study from Viskin and co-workers that same year[5] and large population association studies between 2009 and 2012[6–8].

Genetic mutations in *KCNJ8* leading to a gain of function in ATP-sensitive potassium channel current ($I_{K\text{-}ATP}$)[9–11] or in *CACNA1C, CACNA2D1* and *CACNB2* leading to a loss of function I_{Ca}[12], or in *SCN5A*, leading to a loss of function of I_{Na}[13,14], have been shown to underlie both ERS and BrS.

Here, we report, for the first time, an association of a gain of function in $I_{K\text{-}ATP}$ secondary to mutations in *ABCC9* with ERS and BrS. To our knowledge, this is also the first report of a compound genetic variation in both the cardiac $I_{K\text{-}ATP}$ and I_{Na} giving rise to an overlap syndrome consisting of BrS, ERS, cardiac conduction disease (CCD) and long QT syndrome (LQTS) in a single family.

2. Methods

Informed consent was obtained from all subjects in accordance with local institutional review board guidelines. The investigation conforms to the principles outlined in the Declaration of Helsinki.

2.1. Clinical study

Clinical data, including ECG, clinical history of syncope, seizures, or aborted cardiac arrest, temporally related triggers, and family history, were extracted and maintained in a custom database. Subjects underwent a detailed clinical and cardiovascular examination, including a 12-lead ECG and a 24-hr Holter recording.

The QT interval was measured in lead II or V_5 of the ECG and corrected for heart rate (QTc) using Bazett's formula. Subjects were considered as affected by LQTS if they showed prolongation of the QT interval (QTc ≥ 460 ms) and/or syncope or documented torsade de pointes. BrS was identified on the basis of the presence of ST-segment elevation ≥ 2 mm (≥0.20 mV) in leads V_1 through V_3 at baseline or after administration of intravenous sodium channel blockers (1 mg/kg ajmaline). ERS was identified on the basis of J-point elevation of at least 0.2 mV in the inferior leads (II, III, and aVF), lateral leads (I, aVL, and V_4 to V_6), or both. Phenotypic data were interpreted without knowledge of genotype.

2.2. Genetic sequencing

In this study, 150 unrelated BrS and/or ERS patients and family members were systematically analyzed for laboratory-based BrS and ERS genetic testing. Genomic DNA was prepared from peripheral blood lymphocytes using a commercial kit (Gentra System, Puregene, Valencia, CA, USA). Mutation analysis included direct sequencing of all known LQTS, ERS and BrS susceptibility genes in probands and available family members. Target genes were amplified with intronic primers and sequenced in both directions to probe for mutations, with the use of an ABI PRISM 3100-Avant Automatic DNA sequencer (Applied Biosystem. Foster City, CA, USA). The reference sequence of *ABCC9* and *SCN5A* are shown as NM_005691 and NM_000335 in PubMed. The mutations were performed using the mutagenic sense and antisense primers in Table 1. More than 200 individuals, matched by race and ethnic background (Caucasian), with no history of cardiac arrhythmias, were used as controls.

2.3. Mutagenesis, cell transfection and electrophysiological recordings

Variations (S1402C and V734I) in the regulatory *ABCC9* subunit (human) were introduced in pECE plasmid by PCR amplification of both DNA strands with complementary primers containing the desired amino acid changes (QuickChange, Stratagene, Agilent Technologies, Inc, Santa Clara, CA, USA). HEK293 cells were transiently co-transfected with the wild-type *KCNJ11* pore along with wild-type (WT) or mutant *ABCC9* constructs, and the reporter gene green fluorescent protein with Lipofectamine 2000 reagent (Invitrogen, Carlsbad, CA, USA) according to manufacturer instructions.

Mutant *SCN5A* channel was prepared using the Gene Tailor Site-Directed Mutagenesis System (Invitrogen, Carlsbad, CA, USA) on full length WT *SCN5A* cDNA (hH1c) cloned into pcDNA3.1$^+$ plasmid. Sodium channels were expressed in modified human embryonic kidney cell line TSA201 as previously described[15]. Briefly, TSA201 cells were co-transfected with *SCN5A* (WT, E1784K or WT/E1784K) and *SCN1B* using the Fugene6 method. In addition CD_8 cDNA was co-transfected as reporter gene to visually identify transfected cells by Dynabeads (M-450 CD8 Dynal, Invitrogen, Carlsbad, CA, USA).

Cells were cultured in Dulbecco's Modified Eagle's Medium with 10% FBS and 2 mM glutamine at 5% CO_2. The cells were grown on polylysine coated 35 mm culture dishes and laced in a temperature-controlled chamber at 37°C for 24 to 72 hours, and then studied at room temperature.

2.4. Electrophysiological recordings

Macroscopic currents of $I_{K\text{-}ATP}$ were recorded in the inside-out configurations of the patch-clamp technique[16] using an Axopatch-200B amplifier (Molecular Devices, Sunnyvale, CA, USA). Data acquisition and command potentials were controlled by pClamp 9.0 software (Molecular Devices, Sunnyvale, CA, USA). Patch pipettes with a resistance of 1–2 MΩ were made from borosilicate capillary glass (WPI, Sarasota, FL, USA). To prevent current run-down, inside-out patches were recorded using a fluoride, vanadate and pyrophosphate-potassium solution on both sides of the patch, containing (mM): 123 KCl, 5 K_2EDTA, 7.2 K_2HPO_4, 8 KH_2PO_4, 0.1 Na_3VO_4, 5 KF, 10 $K_4HP_2O_7$ and pH 7.2[17]. The application of 50 mM K_2ATP or MgATP was sufficient to abolish any detectable current through Kir6.2 channels, and off-line subtraction of 50 mM K_2ATP or MgATP currents was used to subtract endogenous currents. A stock solution of K_2ATP or MgATP (Sigma, St. Louis, MO, USA) was prepared and dissolved directly in the bath solution at the desired concentration. Inside-out patches were exposed to ATP solutions until steady-state effects were achieved. For inside-out experiments, currents were normalized to the current recorded at −80 mV under control conditions. The fractional block of current (f) was plotted as a function of drug concentration ([D]) and the data were fit with a Hill equation (1):

$$f=1/\{1+(IC_{50}/[D]^{nh})\} \quad \text{equation (1)}$$

to determine the half-maximal inhibitory concentration (IC_{50}) and the Hill coefficient (nh).

Membrane currents were measured using whole-cell patch-clamp techniques for I_{Na}[15]. All recordings were obtained using an Axopatch 200B amplifier equipped with a CV-201A head stage (Axon Instruments, San Francisco, CA, USA). Measurements were started 10 minutes after obtaining the whole-cell configuration to allow the current to stabilize. Macroscopic whole cell Na^+ current was recorded by using bath solution perfusion containing (in mmol/ L) 140 NaCl, 5 KCl, 1.8 $CaCl_2$, 1 $MgCl_2$, 2.8 Na Acetate, 10 HEPES, and 10 Glucose (pH 7.3 with NaOH). Tetraethylammonium Chloride (5 mmol/ L) was added to the buffer to block TEA-sensitive native currents. Patch pipettes were fabricated from borosilicate glass capillaries (1.5 mm O.D., Fisher Scientific, Pittsburgh, PA, USA). They were pulled using a gravity puller (Model PP-89, Narishige Corp, Tokyo, Japan) to obtain a resistances between 1–2 MΩ when filled with a solution containing (in mmol/L) 5 NaCl, 5 KCl, 130 CsF, 1.0 MgCl2, 5 EGTA and 10 HEPES (pH 7.2 with CsOH). Currents were filtered with a four pole Bessel filter at 5 kHz and digitized at 50 kHz. Series resistance was electronically compensated at 70–85%. The parameters for voltage dependence of activation were estimated from the current voltage relation based on the equation:
$I=G_{max}\cdot(V-V_{rev})/(1+\exp(-(V-V_{1/2})/k)$, where I is the peak current amplitude, G_{max} the maximum conductance, V test potential, V_{rev} the reversal potential, $V_{1/2}$ the midpoint of activation, and k the slope factor. Steady-state availability was fitted to the Boltzmann equation, $I/I_{max}=1/(1+\exp(V-V_{1/2})/k)$ to determine the membrane potential for half-maximal inactivation $V_{1/2}$ and the slope factor k. Recovery from inactivation was analyzed by fitting data to a double exponential function:
$I(t)/I_{max}=A_f\cdot(1-\exp(-t/\tau_f))+As\cdot(1-\exp(-t/\tau_s))$, where A_f and A_s are the fractions of fast and slow inactivating components, respectively, and τ_f and τ_s are their time constants.

All patch-clamp data acquisition and analysis were performed using pCLAMP V10.0 (Axon Instruments, Foster City, CA, USA), EXCEL 2007 (Microsoft, Redmond, WA, USA) and ORIGIN 7.5 (Microcal Software, Northampton, MA, USA).

2.5. Molecular modeling, sequence alignment and topology prediction

A structural model of SUR2A nucleotide binding domains (NBD1/NBD2) was built using the homology modeling program MODELLER 6. The crystal structure of the HlyB-NBD dimer (PDB code: 1XEF) served as a template identified by the FASTA search[18].

SUR2A sequences from human, mouse, rat and rabbit were aligned using ClustalX (http://www.ebi.ac.uk/clustalw). Prediction of transmembrane domain (TMD) helices and topology of the human SUR2A was generated using the hidden Markov model for topology prediction method (http://www.enzim.hu/hmmtop/index.html), in which topology of transmembrane proteins is determined by the maximum divergence of amino acid composition of sequence segments[19]. Human SUR2A was predicted to have 5+6+6 membrane-spanning α-helices grouped in bundles of transmembrane domains TMD0, TMD1, and TMD2 [18].

2.6. Statistical analysis

Continuous variables were reported as mean ± SEM (*n* = number of cells). A comparison between the two and more groups was performed with two-tailed Student's t-test or ANOVA coupled with Student-Newman-Keuls test, as appropriate. $P \leq 0.05$ was considered to indicate statistical significance (SigmaStat, Systat Software, San Jose, CA, USA).

3. Results

3.1. Genetic yield of ABCC9 mutations in BrS and/or ERS probands

In this study of 150 unrelated BrS and/or ERS patients, we identified 8 different mutations in *ABCC9* in 11 probands, providing an overall yield of 7.33% in this population. Excluding 5 cases that also carried mutations in other potentially pathogenic genes (*SCN5A*, *SCN10A*, *CACNA1C*), we obtained a yield of 4.00% for probands carrying only the *ABCC9* genetic variants. None of the variants was found in our >200 ethnically-matched healthy controls. Table 2 summarizes the demographics and genetic screening results for the *ABCC9*-positive patients. All were male with a mean age at time of diagnosis of 34.09 ± 5.09 years. They were highly symptomatic; 81.82% presenting with syncope, 63.64% with sudden cardiac death (SCD), 45.46% showing VT/VF, and 45.46% having a family history of cardiac events or unexplained sudden death.

3.2. Clinical characteristics and genetic analysis of probands with ABCC9-V734I mutation

Four probands were found to carry an *ABCC9*-V734I mutation. The first (Proband 4 in Table 2) was a 20 y/o male. His mother's cousin died at age 20 due to a cardiac arrest secondary to myocardial infarction (MI) and his maternal grandfather's cousin died suddenly at age 25. He experienced palpitations and near syncope since age 16 years and symptoms became more frequent with advancing age. He had a procainamide challenge at a younger age as well as a vagal challenge using carotid sinus massage and Valsalva maneuvers, neither resulted in a Brugada-type pattern. His ECG showed sinus bradycardia, sinus arrhythmia, and typical ER pattern characterized by an elevated J point in leads V2-V6, II, III and aVF (Figure 1A). The second patient (Proband 5 in Table 2) was also a 20 y/o male with family history of arrhythmia and syncope. He presented with VF and was cardioverted. He was initially diagnosed with BrS and then with ERS type 3 (ERS3) and bradycardia (Figure 1B). An implantable cardioverter defibrillator (ICD) was implanted and he subsequently received multiple appropriate shocks. The third patient (Proband 6 in Table 2), a 40 y/o male, presented with sinus bradycardia, 1st degree atrioventricular (AV) block,

ventricular bigeminy (closely-coupled extrasystoles) and a global ER pattern. On the day of admission he had recurrent syncope due to polymorphic VT and sustained VF, which necessitated repetitive external defibrillations. At times, he presented with severe bradycardia that was associated with both coved-type ECG changes in V1 to V3 and also ERS with J waves/point elevation apparent in Leads I, II, aVL, V2-V6, associated with recurrent closely-coupled bigeminy (Figure 1C–1). He was diagnosed as having ERS type 3. With the abolition of bradycardia, first by placement of a temporary pacemaker and then implantation of an ICD, the VF episodes disappeared. No antiarrhythmic drugs were administered at any time during the electrical storm since pacing alone prevented VF (Figure 1C–2). The last case was also a 20 y/o male (Proband 7 in Table 2) with a history of 2 syncopal episodes while exercising. Physical exam was normal, 2D echo revealed mild RA & RV dilation with normal LV and RV ejection fraction. ECGs showed bradycardia (HR 46 bpm) and an ER pattern with notching in the inferior leads, leading to a diagnosis of ERS Type 2 (ECG not shown).

Genetic screening revealed that all four cases had a c.2200G>A transition in exon 17 predicting substitution of an isoleucine for a valine at position 734 of *ABBCC9* (V734I, Figure 2B). A valine at position 734 of *ABCC9* is highly conserved among species (Figure 2C). Proband 6 also had a novel mutation in *SCN5A* due to an insertion of an adenine (A) at nucleotide position 3891, predicting a frameshift and a stop codon (G1297G FSX, Figure 2A). Proband 7 carried P817S mutation in *CACNA1C* as well.

3.3. Functional expression of ABCC9-V734I mutation

Expression studies using inside-out patch clamp techniques to evaluate the effect of the mutation were performed with *ABCC9*-V734I co-expressed with *KCNJ11*-WT. We observed a gain of function in $I_{K\text{-}ATP}$, as a result of a reduced sensitivity of the ATP-sensitive potassium channel (K_{ATP}) to ATP. The IC_{50} value of Mg-ATP for the mutant *KCNJ11*-WT/*ABCC9*-V734I was 5 fold that of WT (97 ± 22 μM for WT, n=5; 510 ± 29 μM for V734I, n=5; Figure 2D & 2E).

Using synchrotron radiation X-ray scattering, we recently demonstrated that when NBD1 V734 is replaced by a larger I residue of SUR2A, it is charted at a loop region distant to either Walker A or Walker B motifs, and the resolved quaternary structure indicates that the afflicted residue is at the juncture between regulatory NBD1/NBD2 domains and the groove for channel protein insertion, demonstrating that I734 clusters at a position critical for protein-protein interaction underlying the structural integrity of the K_{ATP} channel complex [20].

3.4. Clinical characteristics of proband and family members with S1402C mutation

An 18-year-old male (II-1 in Figure 3, Patient 10 in Table 2) presented with two episodes of syncope. The ECG showed QT prolongation and a borderline BrS pattern at baseline. A type-1 ST segment elevation was observed in leads V_1, V_2 and aVR following ajmaline challenge, confirming the diagnosis of BrS (Figure 3E). Sinoatrial block was detected by an implantable loop recorder. The ECG of his father (I-1) displayed a J-point elevation of >0.4 mV in leads II, III, aVF, and >0.3 mV in lead V_6 (Figure 3B). This ER pattern was present at baseline, and there was no change in the ER pattern but slight QTc prolongation following verapamil administration. Frequent premature ventricular beats were observed. The ECG of the proband's asymptomatic mother (I-2) displayed QT prolongation, CCD and BrS confirmed by ajmaline test (Figure 3C). The proband's 16-year-old brother (II-2) was asymptomatic and his ECG was normal (Figure 3D). Echocardiogram of all family members showed normal RV and LV function and no dilatation of the cavities.

3.5. Genetic analysis of proband and family members with ABCC9-S1402C mutation

The Pedigree of Patient 10 in Table 2 is presented in Figure 3A. The proband's mother carried a previously reported *SCN5A* mutation, E1784K, caused by a G5350A transition. The mutation is located at the C-Terminal of the channel protein (Figure 4A and 4B). His father carried a heterozygous C4205G transition in *ABCC9* predicting a missense mutation S1402C. A serine at position 1402 of SUR2A is highly-conserved among species (Figure 4C) and predicted to be damaging by polyphen (0.996) and SIFT (0.00). The variation was absent in >400 alleles from our healthy controls and 1000 Genome Database. The proband inherited both mutations from his parents, whereas his brother carried neither mutation. Clinical and genetic features of the family are summarized in Table 3.

3.6. Functional expression of ABCC9-S1402C mutation

The S1402C missense mutation is located in a highly-conserved region of nucleotide-binding domain (NBD) 2 (Figure 5A and 5B). Furthermore, NBD1/NBD2 dimer homology modeling mapped the S1402C substitution adjacent to the conserved linker and chemical knockout/gene complementation (CKC) motifs (Figure 5C). While unique to ABC transporters the linker motif, located ~20 amino acid residues before the Walker B motif, is essential for adenine nucleotide coordination and hydrolysis[21], the thiol groups of the CKC motif could potentially form a disulfide bond with 1402Cys during dynamic conformational change of NBD2. Thus, the S1402C mutation, due to its vicinity to the linker motifs, may alter nucleotide-dependent plasmalemmal K_{ATP} channel gating.

K_2ATP sensitivity of *KCNJ11*- WT/*ABCC9*-WT channels was compared with that of *KCNJ11*-WT/*ABCC9*-S1402C using excised inside-out patches. Currents were elicited by a 3 s voltage ramp from −80 to +80 mV every 15 seconds from a holding potential of 0 mV. Test solutions were applied to the intracellular membrane surface and currents elicited were almost linear in the range of potentials tested. Figure 6 shows normalized current traces for *KCNJ11*-WT/*ABCC9*-WT (Figure 6A) and *KCNJ11*-WT/*ABCC9*-S1402C (Figure 6B) in control and after exposure to K_2ATP. K_2ATP significantly decreased current amplitude in a concentration-dependent manner. Concentration-response curves for the inhibitory effects of K_2ATP on currents measured at −80 mV in both channels are shown in Figure 6C. The IC_{50} of K_2ATP inhibition of *KCNJ11*-WT/*ABCC9*-WT channels (13.4 ± 5 μM; n = 6) was significantly higher when compared with that of *KCNJ11*-WT/*ABCC9*-S1402C channels (8.5 ± 2 mM; n = 6, $p < 0.05$).

3.7. Functional expression of SCN5A-E1784K mutation

SCN5A-E1784K is a previously reported variant associated with congenital LQTS[22–25], BrS[26–28], and sinus node dysfunction[28]. In the present study, the mutation resulted in LQT3, BrS and CCD in proband 10's mother, and also induced a mixed cardiac disorder (sinoatrial block and BrS) in the proband when it appeared together with the *ABCC9* mutation.

In order to investigate the functional consequences of the mutation in both heterozygous and homozygous expression conditions, we expressed WT, E1784K+WT, and E1784K channels in TSA201 cells. Figure 7A shows the I-V relationship for the three groups recorded using whole-cell patch-clamp techniques. Compared to WT, I_{Na} was moderately, but significantly lower for the heterozygous state (E1784K+WT). When E1784K was expressed alone, the loss of function was more prominent. Maximum current amplitude was 665.1 ± 87.6 pA/pF for WT, 465.8 ± 50.6 pA/pF for E1784K+WT, and 259.5 ± 57.1 pA/pF for E1784K. Peak I_{Na} voltage and activation kinetics were no different E1784K+WT shifted the $V_{1/2}$ of steady-state inactivation to more negative potentials compared with WT (Figure 7B). $V_{1/2}$= −92.5 ± 0.82 mV and k = 5.98 ± 0.30 mV for WT; $V_{1/2}$ = −103.5 ± 1.34 mV and k = 7.14 ±

0.49 mV for E1784K+WT; and $V_{1/2}$ = −110.9 ± 1.93 mV and k = 7.6 ± 0.71 mV for E1784K. There were no differences of recovery kinetics among the 3 groups (τ_f: WT = 4.8 ± 0.66, E1784K+WT = 4.78 ± 0.74, E1784K = 4.85 ± 0.69; τ_s: WT = 33.0 ± 2.91, E1784K +WT = 30.6 ± 2.50, E1784K = 33.1 ± 2.47; n = 11, 7, 10 for each group). However, current decay was significantly faster in E1784K+WT and E1784K compared with WT.

The effect of E1784K on late I_{Na} was also evaluated (Figure 8). Tetrodotoxin (TTX) sensitive currents were compared at the end of a 300-ms depolarization, and values were obtained by subtracting values before and after TTX (Figure 8C). Late I_{Na}, represented as % of peak I_{Na}, was significantly higher for E1784K (1.86% ± 0.24% for E1784K+WT, n=5; 2.01% ± 0.11% for E1784K, n=15), compared with WT (0.14%± 0.02%, n=22; Figure 8A). The absolute value of Late I_{Na} density was 1.30 ± 0.29 pA/pF (n=22) for WT channels, 9.91 ± 2.48 pA/pF (n=5) for E1784+WT and 7.49 ± 1.51 pA/pF (n=10) for E1784 mutant channels (Figure 8B).

4. Discussion

4.1 Role of mutations in ABCC9 in ERS and BrS

Nucleotide sensitivity is a central property underlying energy sensing by K_{ATP} channels. Binding of ATP to the Kir6.2 pore inhibits channel opening, whereas MgADP/ATP interactions with NBDs of SUR2A antagonize ATP-induced pore closure conferring the energy-sensing properties to the K_{ATP} channel complex[29]. The NBD2 of SUR2A harbors an intrinsic ATPase activity that facilitates conformational transitions in the regulatory subunit imparting low or high ATP-sensitivity to the K_{ATP} channel [30]. An increase in MgADP stabilizes SUR2A in a state that reduces Kir6.2 sensitivity to ATP favoring K^+ efflux, leading to membrane hyperpolarization and abbreviation of action potential (AP) duration. In the heart, the MgADP-bound state of SUR2A expands the range for ATP inhibition ($IC_{50} \approx 30$ to 300 μM), which however remains far below actual intracellular ATP levels, even under stress[29]. Upon saturating all ADP-binding sites, at ADP > 300 μM, no further significant reduction in ATP sensitivity can be achieved[29]. Cooperative rather than individual contribution of NBDs gates channel operation as ATP binding to NBD1, supported by hydrolysis at NBD2, is a necessary step in securing structural arrangement of both NBD[30,31]. The outcome on K_{ATP} channel pore state is ultimately determined not by the rate of NBD2-mediated catalysis at SUR2A[31], but on the probability that NBD2 will adopt post- *versus* pre-hydrolytic conformation reflecting cooperative NBD interaction[32,33]. Defects in channel function themselves and/or disturbed nucleotide communication between K_{ATP} channels and an intracellular energy network are envisioned as molecular mechanisms contributing to disease[32]. Thus, mutations that alter nucleotide binding or compromise the cooperative nucleotide-dependent NBD interaction within the regulatory channel subunit, such as S1402C and V734I described in this study, are primary candidates for metabolic sensing deficits underlying cardiac channelopathies. Using synchrotron radiation X-ray scattering, we also demonstrated that V734I can disrupt protein-protein interaction critical for the structural integrity of the K_{ATP} channel complex[20].

K_{ATP} channels are expressed in high-density in metabolically active tissues, and are recognized cellular energy sensors[33]. K_{ATP} channels are assembled by the pore-forming inwardly-rectifying potassium Kir6.x channel and the regulatory sulfonylurea receptor SURx, a member of the ATP-binding cassette superfamily. Kir6.2/Kir6.1 (*KCNJ11/KCNJ8*) and SUR2A/SUR1 (*ABCC9/ABCC8*) isoforms in a 4:4 stoichiometry, comprise the cardiac K_{ATP} channel. SUR2A, like other *ABCC* proteins, consists of two bundles of six hydrophobic TMDs fused to hydrophilic NBDs (TMD_1-NBD1-TMD_2-NBD2; Figure 5). An additional TMD_0 module with 5 TMDs (TMD_0-TMD_1-NBD1-TMD_2-NBD2) anchors the

channel pore to the SUR module[34]. Mutations that alter nucleotide binding or compromise the cooperative nucleotide-dependent NBD interaction within the regulatory channel subunit, such as the S1402C and V734I described in this study, are primary candidates for metabolic sensing deficits underlying cardiac. Using synchrotron radiation X-ray scattering, we recently demonstrated that V734I of SUR2A can disrupt protein-protein interaction critical for the structural integrity of the K_{ATP} channel complex[20].

ABCC9 mutations have been reported to be associated with atrial fibrillation, dilated cardiomyopathy with tachycardia, and to influence susceptibility to MI in the human heart[34]. In a cohort of patients with MI at an early age, a rare missense variant V734I in the *ABCC9* gene was found to be over-represented[35]. Statistical significance was demonstrated after controlling for multiple established risk factors for coronary artery disease. Thus far, the only K_{ATP} channel mutation associated with ERS and BrS was in *KCNJ8*-S422L. This was first reported by Haïssaguerre and co-worker in 2009[9], and the effect of this mutation to cause a gain of function of $I_{K\text{-}ATP}$ was reported in 2010[10]. In 2011, we used inside-out patch clamp studies to demonstrate that this mutation produces a gain of function in $I_{K\text{-}ATP}$ by reducing the sensitivity of the K_{ATP} channel to ATP[11]. The rationale for targeting *ABCC9* as a BrS and ERS susceptibility gene stems from our observation a decade ago that pinacidil, an $I_{K\text{-}ATP}$ opener, is capable of inducing these phenotypes in coronary-perfused canine ventricular wedge preparations[1]. Moreover, we and others have recently demonstrated that genetic variants in *KCNJ8* leading to a gain of function in $I_{K\text{-}ATP}$, underlie both ERS and BrS as described above[9–11], We therefore hypothesized that the ATP-sensing subunit (SUR2A) may play an equally important role in these syndromes. In the present study, we report for the first time, the association of BrS and ERS with variants in *ABCC9* capable of causing a gain of function in $I_{K\text{-}ATP}$.

A gain of function in $I_{K\text{-}ATP}$ secondary to a mutation in *ABCC9*, V734I, was also found to be associated with an ERS phenotype in probands 4 to 7 in Table 2. With this finding, our study expands the spectrum of *ABCC9*-V734I variant beyond MI-related arrhythmogenesis, demonstrating its association with ERS-mediated ventricular arrhythmias. All cases were symptomatic males with ERS and bradycardia. Three of them displayed characteristics of ERS Type 3 (ERS3), which is considered by some to be a variant of BrS[36]. It is tempting to speculate that ERS3, which is often associated with electrical storms, involves defects in genes traditionally predisposed to causing BrS, such as *SCN5A*, in addition to mutations in $I_{K\text{-}ATP}$ genes.

Interestingly, a recent study reported that V734I reduced the sensitivity of Kir6.2/SUR2B channels but not of Kir6.2/SUR2A or Kir6.1/SUR2B channels, to MgATP inhibition[37]. The methodology employed was similar to that used in our study in which the mutant produced a significant gain of function of $I_{K\text{-}ATP}$. We used the same expression system (HEK293 cells) and same methodology (inside-out patch), but their solutions were different and vanadate was not used to prevent run-down. Another important difference was their use of rat rather than human plasmids. Also noteworthy is the fact that they found that WT-SUR2A+Kir6.2 channels are significantly more sensitive to Mg-ATP than WT-SUR2B +Kir6.2 channels, opposite from previous studies[38–41].

Proband 10's father, harboring the *ABCC9* mutation, exhibited an ERS phenotype and his mother, harboring the *SCN5A* mutation displayed a combined LQTS and BrS phenotype. Interestingly, the proband, having inherited both mutations, displayed BrS and CCD phenotypes, but not the LQTS or ERS phenotype. The combination may have facilitated the appearance of a more severe BrS phenotype at a relatively young age (18 y/o vs. an average of 40 y/o) since both contribute to an outward shift in the balance of current in the early phase of the AP, which is known to underlie the development of the electrocardiographic

and arrhythmic manifestations of BrS. The absence of the LQTS phenotype in the proband may also be due to an effect of the *ABCC9* mutation to boost repolarizing currents via a gain of function in $I_{K\text{-}ATP}$ later in the AP, thus countering the effect of the *SCN5A* mutation to promote late I_{Na}.

The more severe phenotype of Proband 6 than Proband 10, both of whom had defects in *ABCC9* as well as *SCN5A*, may be attributable to the much shorter QTc in Proband 6 (361 vs. 436 ms), thus possibly facilitating the development of closely-coupled extrasystoles via a phase 2 reentry mechanism. The longer QTc in proband 10 is likely due to the gain of function in late I_{Na} associated with the E1784K missense mutation in *SCN5A*.

4.2. SCN5A in CCD, BrS and LQTS

SCN5A mutations are known to cause CCD, BrS or LQTS, in some cases producing an overlap syndrome exhibiting mixed phenotypes. A schematic representation of the cellular changes thought to underlie the Brugada phenotype caused by a loss of function of I_{Na} is shown in Figure 7. Under baseline conditions, ST segment is isoelectric because of the absence of transmural voltage gradient at the level of the AP plateau (left panel of Figure 7D–E). Loss of function in peak I_{Na} accentuates the right ventricular AP notch, leading to exaggeration of transmural voltage gradients and thus to accentuation of the J wave or ST segment elevation. Accentuation of the notch is often accompanied by a prolongation of the epicardial AP such that the direction of the repolarization across the right ventricular wall and transmural voltage gradients are reversed, thus leading to inversion of the T wave. These cellular changes lead to the development of the coved-type (Type 1) ST segment elevation and inverted T wave, typically observed in ECG of the Brugada patients (right panel of Figure 7D–E). The significant loss of function secondary to *SCN5A* mutations, likely contributed to the ST segment elevation in the right precordial leads of Probands 6 and 10. In the case of Proband 10 this was manifest as a BrS phenotype, whereas in Proband 6, the electrocardiographic signature was one of ERS3 with spontaneous VF[1].

The *SCN5A*-E1784K mutation carried by Proband 10 was shown to significantly increase late I_{Na} leading to a LQTS phenotype. Figure 8D–E schematically illustrates the cellular changes contributing to QT prolongation.

5. Limitations and Conclusions

We did not conduct functional expression studies on *SCN5A*-G1297G FSX22, but the electrophysiological consequence of this mutation could be reasonably deduced, based on the predicted stop codon leading to truncation and a non-functional protein. We do not claim that all of the variants found in this study are causative of the respective syndromes. Clearly, additional studies are needed to determine pathogenicity. Investigations of the functional consequence of combined *ABCC9* and *SCN5A* variations are not available and would be most welcome in the form of studies involving transgenic animal or other *in vivo* models. We are working on advancing our understanding of the influence of *ABCC9* mutations by generating induced pluripotent stem cell-derived cardiomyoctyes generated by reprogramming of fibroblasts isolated from BrS and ERS patients[42]. This technology will make it possible to assess the effects of mutations in the context of all the other variants in the patient's genome, and to record from cardiac cells that contain tissue-specific accessory proteins and splice variants not available in heterologous test systems.

The present study provides, for the first time, evidence in support of the hypothesis that *ABCC9* is an ERS and BrS susceptibility gene with clear male-dominance. An *ABCC9*-S1402C missense mutation, highly conserved among species and absent in >200 ethnically-matched controls, and a previously reported MI-related *ABCC*9-V734I mutation, are shown

to cause a significant gain of function in K_{ATP} current when co-expressed in a heterologous expression system and evaluated using inside-out patch clamp experiments. We also provide the first report of a compound genetic variation in $I_{K\text{-}ATP}$ and I_{Na} (loss of function in peak I_{Na}^{+} gain of function in late I_{Na}) giving rise to an overlap syndrome consisting of BrS, ERS, CCD and LQTS in the same family. Finally, we demonstrate an association of ERS3 with a combination of gain of function mutation in $I_{K\text{-}ATP}$ and a loss of function mutation in I_{Na}, resulting in a severe arrhythmogenic phenotype.

The overall yield for *ABCC9* mutations in JWS approaches 7.33% in our study population. All *ABCC9*-positive cases were males who presented with a high prevalence of syncope, SCD, and VT/VF. R1197C was identified as a newly-identified mutation and V734I was the most frequently encountered variant.

Acknowledgments

This work was supported by National Institute of Health [HL47678] to CA; NYSTEM [C026424] to CA; SEP CONACYT [CB-2008-01-105941] to J.A.C.; CONACYT [FM (201866)] to HBM and DH; and the Masons of New York, Florida, Massachusetts Connecticut, Maryland, Rhode Island and Wisconsin.

The authors are grateful to Judy Hefferon for technical assistance and Susan Bartkowiak for maintaining the MMRL's Genetic Database. We also wish to acknowledge the contribution of Lee Arnold Biblo, M.D. of the Medical College of Wisconsin.

All authors of this manuscript have certified that they comply with the *Principles of Ethical Publishing* in the International Journal of Cardiology.

References

1. Antzelevitch C, Yan GX. J wave syndromes. Heart Rhythm. 2010; 7:549–58. [PubMed: 20153265]
2. Mehta MC, Jain AC. Early repolarization on scalar electrocardiogram. Am J Med Sci. 1995; 309:305–11. [PubMed: 7771499]
3. Haissaguerre M, Derval N, Sacher F, Jesel L, Deisenhofer I, De Roy L, et al. Sudden cardiac arrest associated with early repolarization. N Engl J Med. 2008; 358:2016–23. [PubMed: 18463377]
4. Nam GB, Kim YH, Antzelevitch C. Augmentation of J waves and electrical storms in patients with early repolarization. N Engl J Med. 2008; 358:2078–9. [PubMed: 18463391]
5. Rosso R, Kogan E, Belhassen B, Rozovski U, Scheinman MM, Zeltser D, et al. J-point elevation in survivors of primary ventricular fibrillation and matched control subjects: incidence and clinical significance. J Am Coll Cardiol. 2008; 52:1231–8. [PubMed: 18926326]
6. Tikkanen JT, Anttonen O, Junttila MJ, Aro AL, Kerola T, Rissanen HA, et al. Long-term outcome associated with early repolarization on electrocardiography. N Engl J Med. 2009; 361:2529–37. [PubMed: 19917913]
7. Noseworthy PA, Tikkanen JT, Porthan K, Oikarinen L, Pietila A, Harald K, et al. The early repolarization pattern in the general population clinical correlates and heritability. J Am Coll Cardiol. 2011; 57:2284–9. [PubMed: 21600720]
8. Tikkanen JT, Wichmann V, Junttila MJ, Rainio M, Hookana E, Lappi OP, et al. Association of early repolarization and sudden cardiac death during an acute coronary event. Circ Arrhythm Electrophysiol. 2012; 5:714–8. [PubMed: 22730409]
9. Haissaguerre M, Chatel S, Sacher F, Weerasooriya R, Probst V, Loussouarn G, et al. Ventricular fibrillation with prominent early repolarization associated with a rare variant of KCNJ8/K_{ATP} channel. J Cardiovasc Electrophysiol. 2009; 20:93–8. [PubMed: 19120683]
10. Medeiros-Domingo A, Tan BH, Crotti L, Tester DJ, Eckhardt L, Cuoretti A, et al. Gain-of-function mutation S422L in the KCNJ8-encoded cardiac K(ATP) channel Kir6. 1 as a pathogenic substrate for J-wave syndromes. Heart Rhythm. 2010; 7:1466–71. [PubMed: 20558321]

11. Barajas-Martinez H, Hu D, Ferrer T, Onetti CG, Wu Y, Burashnikov E, et al. Molecular genetic and functional association of Bugada and early repolarization syndromes with S422L missense mutation in KCNJ8. Heart Rhythm. 2012; 9:548–55. [PubMed: 22056721]
12. Burashnikov E, Pfeiffer R, Barajas-Martinez H, Delpon E, Hu D, Desai M, et al. Mutations in the cardiac L-type calcium channel associated J wave sydnrome and sudden cardiac death. Heart Rhythm. 2010; 7:1872–82. [PubMed: 20817017]
13. Hu D, Barajas-Martinez H, Pfeiffer R, Burashnikov E, Caceres G, Antzelevitch C. The role of SCN5A mutations in J wave syndromes. Circulation. 2010; 122:A18124. Abstract.
14. Watanabe H, Nogami A, Ohkubo K, Kawata H, Hayashi Y, Ishikawa T, et al. Electrocardiographic characteristics and SCN5A mutations in idiopathic ventricular fibrillation associated with early repolarization. Circ Arrhythm Electrophysiol. 2011; 4:874–81. [PubMed: 22028457]
15. Hu D, Barajas-Martinez H, Burashnikov E, Springer M, Wu Y, Varro A, et al. A mutation in the beta 3 subunit of the cardiac sodium channel associated with Brugada ECG phenotype. Circ Cardiovasc Genet. 2009; 2:270–8. [PubMed: 20031595]
16. Hamill OP, Marty A, Neher E, Sakmann B, Sigworth FJ. Improved patch-clamp techniques for high-resolution current recording from cells and cell-free membrane patches. Pflugers Arch. 1981; 391:85–100. [PubMed: 6270629]
17. Huang CL, Feng S, Hilgemann DW. Direct activation of inward rectifier potassium channels by PIP2 and its stabilization by Gbetagamma. Nature. 1998; 391:803–6. [PubMed: 9486652]
18. Park S, Lim BB, Perez-Terzic C, Mer G, Terzic A. Interaction of asymmetric ABCC9-encoded nucleotide binding domains determines KATP channel SUR2A catalytic activity. J Proteome Res. 2008; 7:1721–8. [PubMed: 18311911]
19. Tusnady GE, Simon I. Principles governing amino acid composition of integral membrane proteins: application to topology prediction. J Mol Biol. 1998; 283:489–506. [PubMed: 9769220]
20. Park S, Terzic A. Quaternary structure of KATP channel SUR2A nucleotide binding domains resolved by synchrotron radiation X-ray scattering. J Struct Biol. 2010; 169:243–51. [PubMed: 19919849]
21. Higgins CF, Linton KJ. The ATP switch model for ABC transporters. Nat Struct Mol Biol. 2004; 11:918–26. [PubMed: 15452563]
22. Wei J, Wang DW, Alings M, Fish F, Wathen M, Roden DM, et al. Congenital long-QT syndrome caused by a novel mutation in a conserved acidic domain of the cardiac Na+ channel. Circulation. 1999; 99:3165–71. [PubMed: 10377081]
23. Deschênes I, Baroudi G, Berthet M, Barde I, Chalvidan T, Denjoy I, et al. Electrophysiological characterization of *SCN5A* mutations causing long QT (E1784K) and Brugada (R1512W and R1432G) syndromes. Cardiovasc Res. 2000; 46:55–65. [PubMed: 10727653]
24. Tester DJ, Will ML, Haglund CM, Ackerman MJ. Compendium of cardiac channel mutations in 541 consecutive unrelated patients referred for long QT syndrome genetic testing. Heart Rhythm. 2005; 2:507–17. [PubMed: 15840476]
25. Nakajima T, Kaneko Y, Saito A, Irie T, Tange S, Iso T, et al. Identification of six novel SCN5A mutations in Japanese patients with Brugada syndrome. Int Heart J. 2011; 52:27–31. [PubMed: 21321465]
26. Priori SG, Napolitano C, Schwartz PJ, Bloise R, Crotti L, Ronchetti E. The elusive link between LQT3 and Brugada syndrome: the role of flecainide challenge. Circulation. 2000; 102:945–7. [PubMed: 10961955]
27. Priori SG, Napolitano C, Gasparini M, Pappone C, Della BP, Giordano U, et al. Natural history of Brugada syndrome: insights for risk stratification and management. Circulation. 2002; 105:1342–7. [PubMed: 11901046]
28. Makita N, Behr E, Shimizu W, Horie M, Sunami A, Crotti L, et al. The E1784K mutation in SCN5A is associated with mixed clinical phenotype of type 3 long QT syndrome. J Clin Invest. 2008; 118:2219–29. [PubMed: 18451998]
29. Selivanov VA, Alekseev AE, Hodgson DM, Dzeja PP, Terzic A. Nucleotide-gated KATP channels integrated with creatine and adenylate kinases: amplification, tuning and sensing of energetic signals in the compartmentalized cellular environment. Mol Cell Biochem. 2004; 256–257:243–56.

30. Park S, Lim BB, Perez-Terzic C, Mer G, Terzic A. Interaction of asymmetric ABCC9-encoded nucleotide binding domains determines KATP channel SUR2A catalytic activity. J Proteome Res. 2008; 7:1721–8. [PubMed: 18311911]

31. Zingman LV, Hodgson DM, Bienengraeber M, Karger AB, Kathmann EC, Alekseev AE, et al. Tandem function of nucleotide binding domains confers competence to sulfonylurea receptor in gating ATP-sensitive K+ channels. J Biol Chem. 2002; 277:14206–10. [PubMed: 11825892]

32. Bienengraeber M, Olson TM, Selivanov VA, Kathmann EC, O'Cochlain F, Gao F, et al. ABCC9 mutations identified in human dilated cardiomyopathy disrupt catalytic K_{ATP} channel gating. Nat Genet. 2004; 36:382–7. [PubMed: 15034580]

33. Alekseev AE, Hodgson DM, Karger AB, Park S, Zingman LV, Terzic A. ATP-sensitive K+ channel channel/enzyme multimer: metabolic gating in the heart. J Mol Cell Cardiol. 2005; 38:895–905. [PubMed: 15910874]

34. Terzic A, Alekseev AE, Yamada S, Reyes S, Olson TM. Advances in cardiac ATP-sensitive K+ channelopathies from molecules to populations. Circ Arrhythm Electrophysiol. 2011; 4:577–85. [PubMed: 21846889]

35. Minoretti P, Falcone C, Aldeghi A, Olivieri V, Mori F, Emanuele E, et al. A novel Val734Ile variant in the ABCC9 gene associated with myocardial infarction. Clin Chim Acta. 2006; 370:124–8. [PubMed: 16563363]

36. Kalla H, Yan GX, Marinchak R. Ventricular fibrillation in a patient with prominent J (Osborn) waves and ST segment elevation in the inferior electrocardiographic leads: a Brugada syndrome variant? J Cardiovasc Electrophysiol. 2000; 11:95–8. [PubMed: 10695469]

37. Smith KJ, Chadburn AJ, Adomaviciene A, Minoretti P, Vignali L, Emanuele E, et al. Coronary spasm and acute myocardial infarction due to a mutation (V734I) in the nucleotide binding domain 1 of ABCC9. Int J Cardiol. 2013; 168:3506–13. [PubMed: 23739550]

38. Isomoto S, Kondo C, Yamada M, Matsumoto S, Higashiguchi O, Horio Y, et al. A novel sulfonylurea receptor forms with BIR (Kir6. 2) a smooth muscle type ATP-sensitive K+ channel. J Biol Chem. 1996; 271:24321–4. [PubMed: 8798681]

39. Hambrock A, Loffler-Walz C, Kloor D, Delabar U, Horio Y, Kurachi Y, et al. ATP-Sensitive K+ channel modulator binding to sulfonylurea receptors SUR2A and SUR2B: opposite effects of MgADP. Mol Pharmacol. 1999; 55:832–40. [PubMed: 10220561]

40. Schwanstecher M, Sieverding C, Dorschner H, Gross I, guilar-Bryan L, Schwanstecher C, et al. Potassium channel openers require ATP to bind to and act through sulfonylurea receptors. EMBO J. 1998; 17:5529–35. [PubMed: 9755153]

41. Shindo T, Yamada M, Isomoto S, Horio Y, Kurachi Y. SUR2 subtype (A and B)-dependent differential activation of the cloned ATP-sensitive K+ channels by pinacidil and nicorandil. Br J Pharmacol. 1998; 124:985–91. [PubMed: 9692785]

42. Takahashi K, Yamanaka S. Induction of pluripotent stem cells from mouse embryonic and adult fibroblast cultures by defined factors. Cell. 2006; 126:663–76. [PubMed: 16904174]

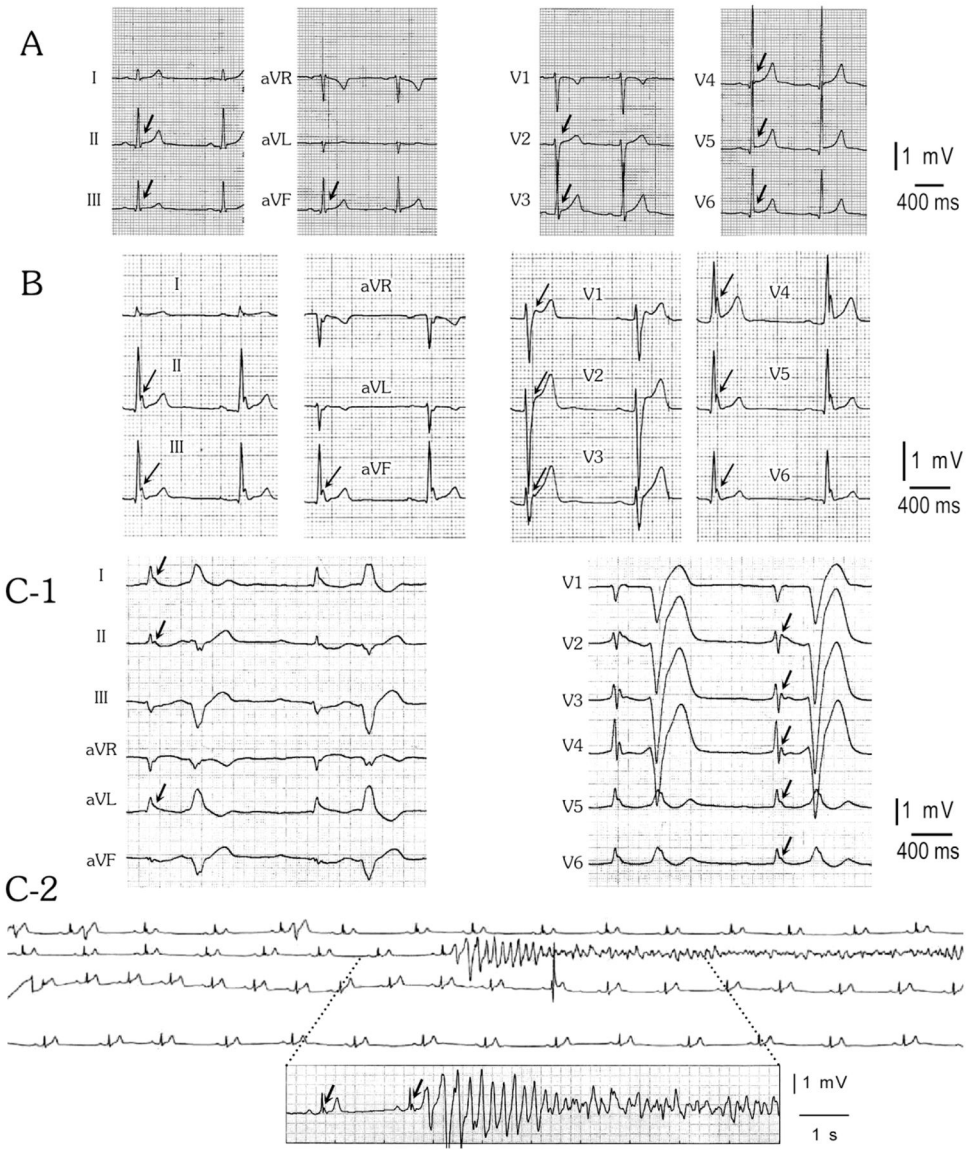

Figure 1. Electrocardiograms (ECGs) of *ABCC9*-V734I variant carriers (Proband 4, 5 and 6 in Table 2)

A and B: The ECG of first and second proband both showed sinus bradycardia and typical global J wave elevation as arrows indicated. **C-1**: ECG of third proband displayed 1st degree atrioventricular block, ventricular bigeminy and an early repolarization pattern including prominent distinct J waves. **C-2:** Ventricular tachycardia/ventricular fibrillation (VT/VF) in the proband was precipitated by a closely coupled premature beat. Polymorphic VT degenerated into VF and was terminated by an appropriate implantable cardioverter defibrillator discharge. Arrows denote prominent J waves.

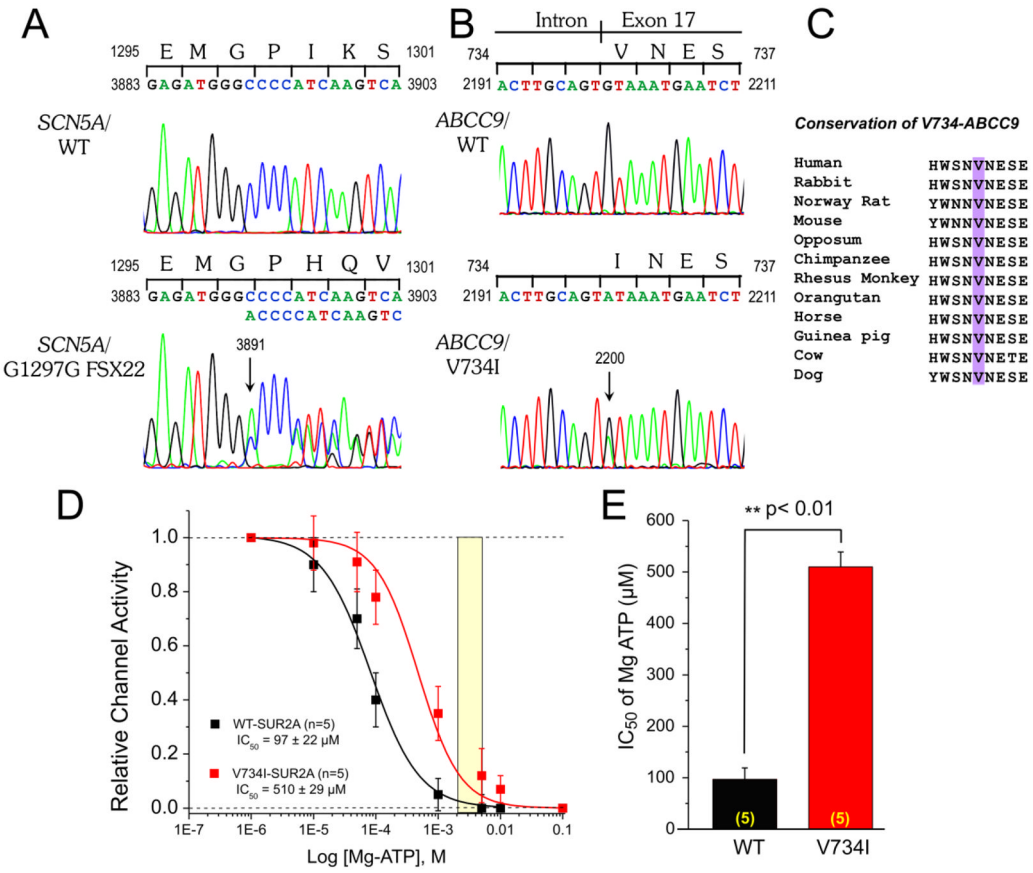

Figure 2. *ABCC9*-V734I mutation causes a gain of function in ATP-sensitive potassium channel (K_{ATP}) activity by reducing sensitivity of K_{ATP} channels to ATP

A: Chromatogram showing a heterozygous A insertion at nucleotide 3891 (exon 22) of *SCN5A*, predicting G1297G FSX22, a stop codon and truncation of $Na_v1.5$ protein. **B:** Chromatogram showing a heterozygous G-to-A transition at nucleotide 2200 (exon 17) in *ABCC9*, predicting a substitution of Isoleucine (I) for Valine (V) at residue 734 (V734I). **C:** Amino acid alignment performed using GenBank accession numbers corresponding to protein sequences shows that a Valine at position 734 is highly conserved among species. **D:** Sensitivity to ATP of *KCNJ11*-wild type (WT)/*ABCC9*-WT and *KCNJ11*-WT/*ABCC9*-V734I channels measured using an excised inside-out patch. **E:** Graph depicting IC_{50} for Mg-ATP inhibition of $I_{K\text{-}ATP}$ for WT- and V734I-*ABCC9* channels. Mean ± SEM. **p<0.01 vs. WT.

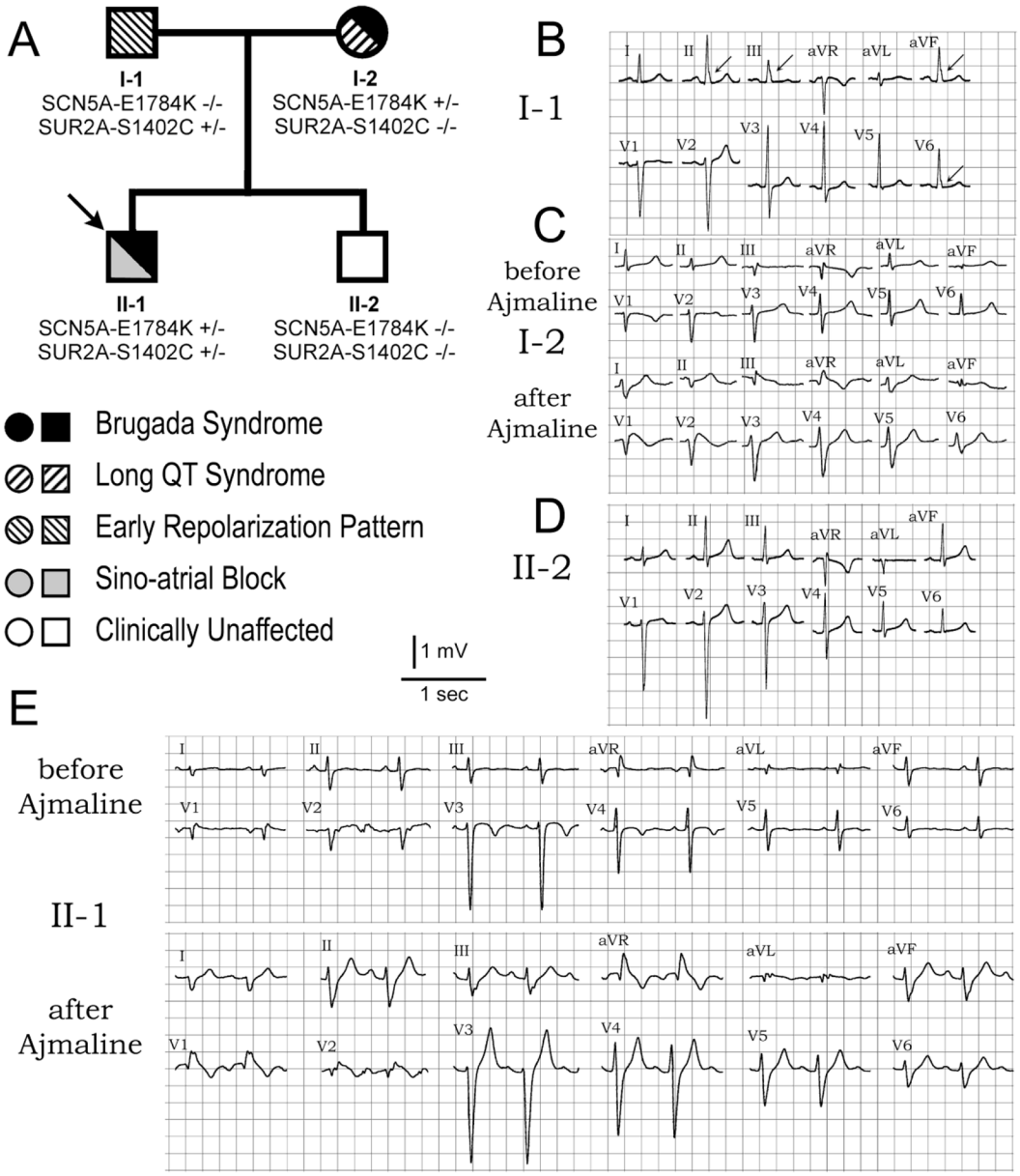

Figure 3. Pedigree and representative electrocardiogram (ECG) tracings of proband 1 and affected family members

A: The family pedigree of BS094. Circles represent female subjects and squares represent male subjects. The arrow denotes the proband. −/− wild type (WT); +/− heterozygous for the mutation. Brugada, long QT, early repolarization (ER) syndromes, sinoatrial block are labeled by black, upward diagonal, downward diagonal, and dark grey symbol; unaffected subject is shown as white. **B:** 12-lead ECG of proband's father (I-1) showing accentuation of ER pattern (arrows) in lead II, III, aVF and V_6. **C:** ECG of the proband's mother before and after ajmaline (I-2); QT and QTc intervals are prolonged. **D:** ECG of proband's younger brother (II-2) is normal. **E:** ECG of proband-1 recorded before and after ajmaline (II-1); ECG shows accentuation of r′ and development of a type 1 ST segment elevation in V_1 and V_2 after ajmaline; QT and QTc are normal.

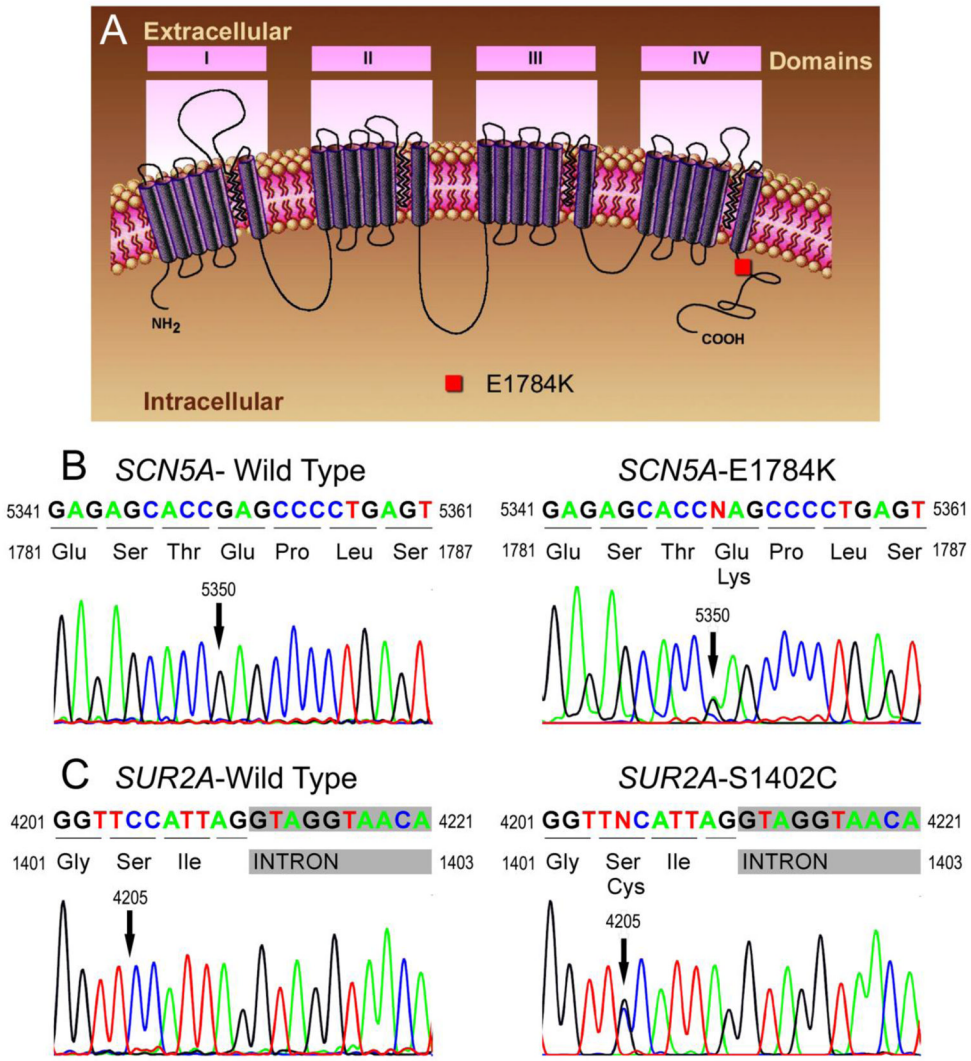

Figure 4. Genetic analysis of proband 1 and the affected family members

A: Human *SCN5A* proposed secondary structure showing the location of theE1784K mutation in the C-terminal of the channel. **B:** PCR-based sequence of *SCN5A* exon 28 showing wild type (WT) and heterozygous G to A transversion at nucleotide 5350 (arrow) in patient I-2 and II-1. The mutation predicts a substitution of Lys (AAG) for Glu (GAG) at position 1784 (E1784K). **C:** Sequence analysis of exon 34 of *ABCC9* in patient I-1 and II-1, showing the heterozygous C to G transversion at nucleotide 4205 (arrow), predicting a substitution of cysteine (TGC) for serine (TCC) at position 1402 (S1402C).

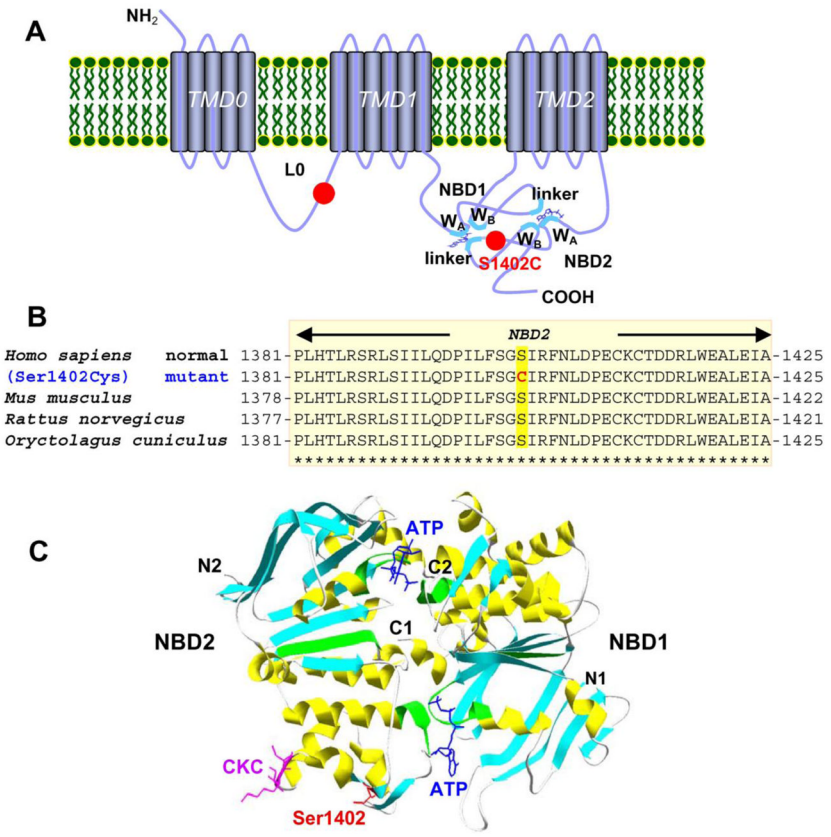

Figure 5. S1402C mutation in *ABCC9*

A: Location of S1402C mutation in SUR2A structure within nucleotide binding domain (NBD) 2 is indicated by red dot. W_A and W_B denote the conserved Walker motifs within ABC protein family that are critical for nucleotide binding. **B:** Alignment of the human SUR2A Ser1402 and surrounding region with orthologs from other species revealed that the mutation located within a highly conserved region. **C:** Homology structural model of the NBD1/NBD2 heterodimer maps S1402C mutation to the region adjacent to the conserved NBD2 linker and CKC motifs. N- and C-termini of individual NBDs. Yellow denotes α-helix, cyan β-strand, green Walker A or B motif (WA or WB) or linker motif, blue ATP, magenta chemical knockout/gene complementation motif, and red Ser1402.

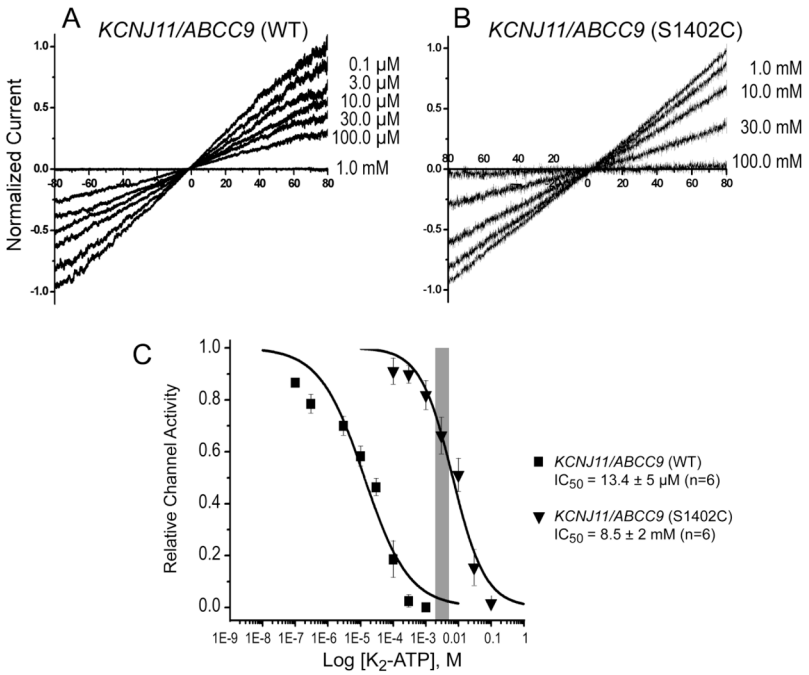

Figure 6. ***ABCC9*-S1402C mutation reduces sensitivity of ATP-sensitive potassium channel (K_{ATP}) to ATP**

A and B: $I_{K\text{-}ATP}$ traces recorded from excised, inside-out macropatches, elicited by applying ramps from −80 to +80 mV (duration, 3 s), before and after attaining steady-state inhibition with K_2ATP. Currents were normalized to the current recorded at −80 mV under control conditions. **C:** Concentration-response curves for the effects of K_2ATP on *KCNJ11*-wild type (WT)/*ABCC9*-WT and *KCNJ11*-WT/*ABCC9*-S1402C mutant channels. Currents were measured at −80 mV. The half-maximal inhibitory concentration (IC_{50}) value of K_2ATP with *KCNJ11*-WT/*ABCC9*-WT (13.4 ± 5 μM; n = 6) was significantly higher for the *KCNJ11*-WT/*ABCC9*-S1402C mutant channel (8.5 ± 2 mM; n = 6, $p < 0.05$).

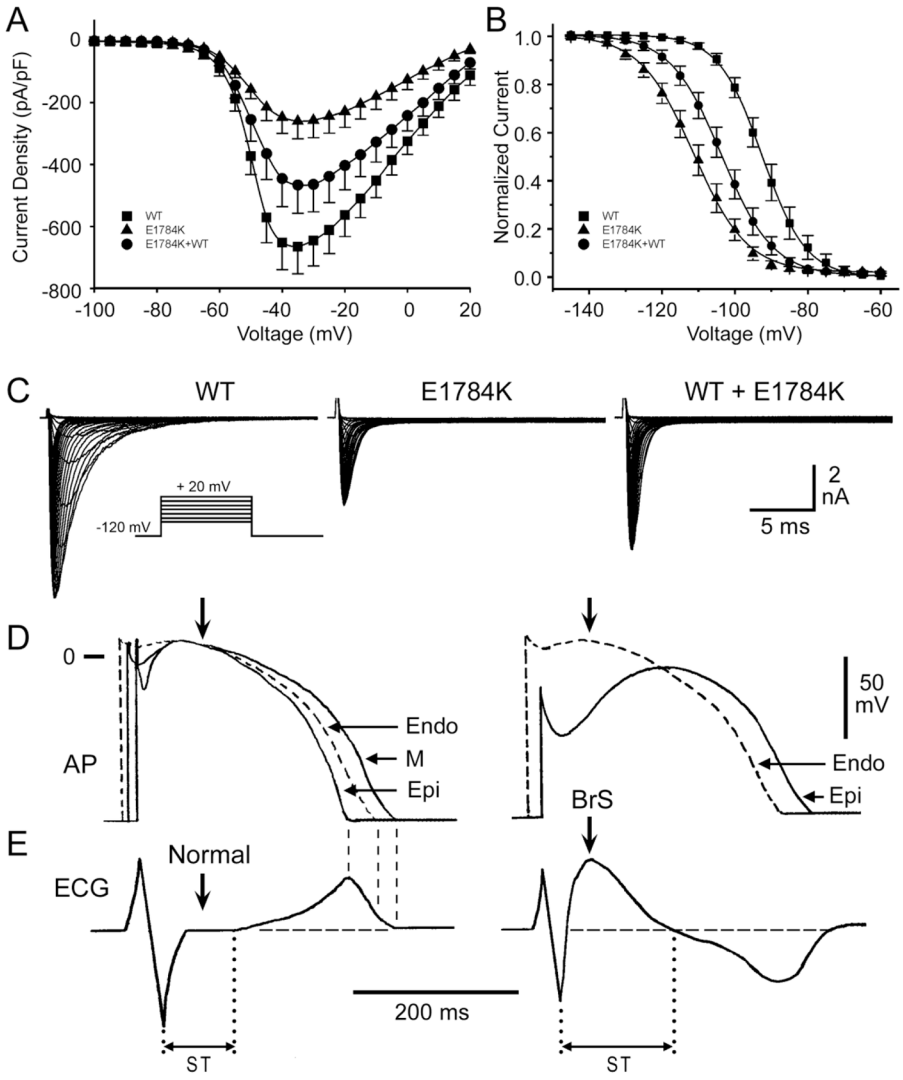

Figure 7. *SCN5A*-E1784K mutation leads to a loss of function of $I_{Na,peak}$, thus inducing a Brugada syndrome phenotype

A: Current-voltage relationship for wild type (WT) (squares, n = 22), E1784K (triangles, n = 23), and E1784K+WT (circles, n = 18). Peak E1784K+WT and E1784K current at −35 mV decreased 30.0% and 61.0% relative to WT, respectively (P <0.05 and P <0.01). **B:** Voltage-dependent channel inactivation for WT (squares, n = 22), E1784K (triangles, n =17) and E1784K+WT (circles, n = 7). Peak current was normalized to their respective maximum values and plotted against the conditioning potential. Data were fitted by Boltzman function. Steady-state inactivation of E1784K and E1784K+WT was 18.4 mV and 11.0 mV more negative than WT (p < 0.01 and 0.01). **C–E:** Whole-cell representative peak currents of *SCN5A*-WT and/or *SCN5A*-E1784K (**panel C**) shows the decreased peak I_{Na} current, proposed to underlie the action potential (AP) changes (**panel D**) and the electrocardiogram (ECG) manifestation (**panel E**) of Brugada syndrome (BrS). Endo: endocardial; Epi: epicardial. Traces in panels D and E are diagrammatic.

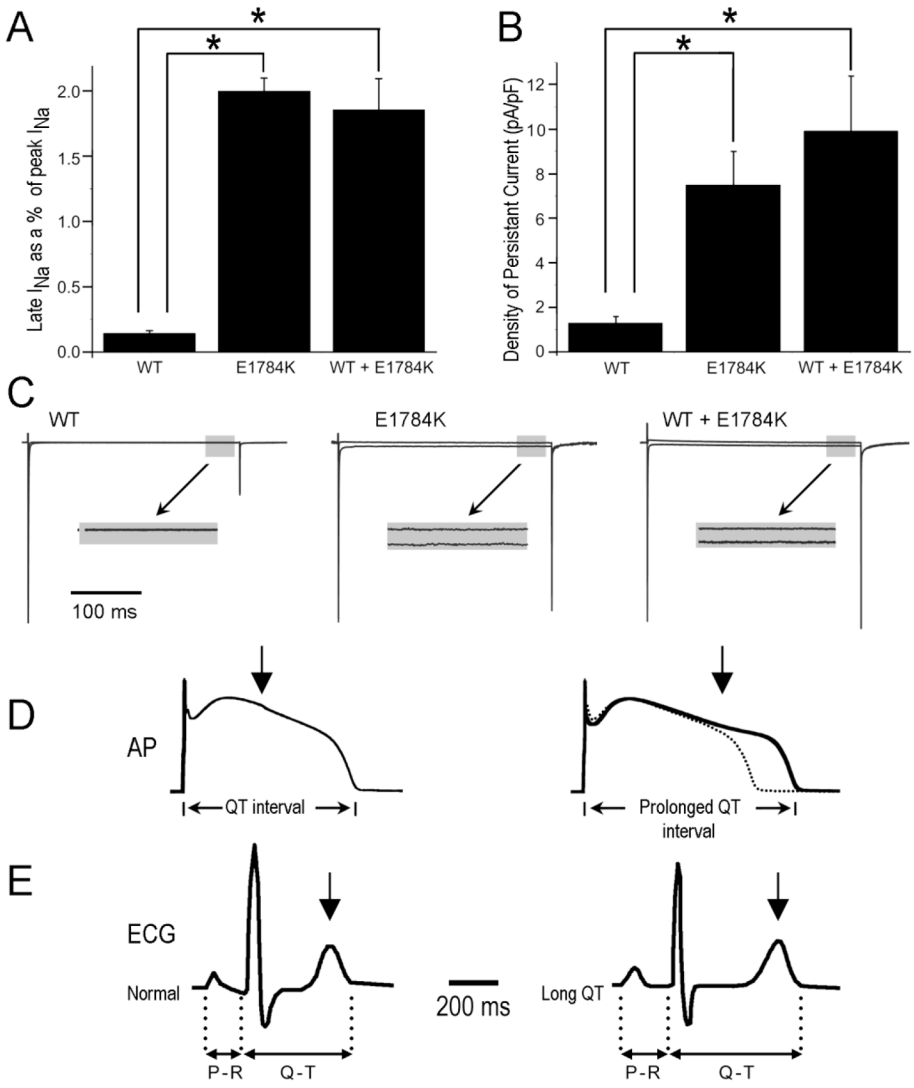

Figure 8. *SCN5A*-E1784K mutation leads to a gain of function of $I_{Na,late}$, thus inducing a long QT syndrome phenotype

A–B: Bar graph of relative $I_{Na,late}$ (% of $I_{Na,peak}$) and $I_{Na,late}$ density (pA/pF) among 3 groups. Statistically significant differences (**P*<0.05) are observed between E1784K+wild type (WT)/E1784K and WT in both panels (*n* = 22, 15, 5 for WT, E1784K and E1784K +WT). $I_{Na,late}$ was 0.14%, 2.01% and 1.86% of $I_{Na,peak}$ in WT, E1784K and E1784K+WT (n =22, 15 and 5). **C–E:** Whole-cell late currents of *SCN5A*-WT and/or *SCN5A*-E1784K (**panel C**) showing a larger $I_{Na,late}$ for the mutant channel and its effect to prolong action potential (AP) duration (**panel D**) and QT interval (**panel E**), which cause LQTS-3. ECG: electrocardiogram. $I_{Na,peak}$ in panel C is normalized to the same level; traces in panels D and E are diagrammatic.

Table 1

Sequences of primers for genetic variants in *SCN5A* and *ABCC9*.

Gene	Exon	Sense	Antisense
SCN5A	22	5′-CCA GAA GGC CTA CTG TCT GTC-3′	5′-CAT AGG ACA TCA GAA GCA CAG G-3′
SCN5A	28	5′-AAG TGG GAG GCT GGC ATC GAC-3′	5′-GTC CCC ACT CAC CAT GGG CAG-3′
ABCC9	17	5′-GAG CAG GGT TAG CAC TAG AAC-3′	5′-CAG TTG ACA CAA GGA GCC AC-3′
ABCC9	34	5′-CTG CTC TGG GCA CTG TTC TAG-3′	5′-GTT ACT GGG TTC ACC CTC TTG-3′

Table 2

Clinical and genetic characteristics of *ABCC9* affected probands.

	General Information					Symptom			Treatment	Other suspected genes	*ABCC9*						
Proband No.	**Age for Dx (y/o)**	**Gender**	**Dx**	**VT/VF**	**FH***	**Syncope**	**SCD**	**Other****			**Name**	**SIFT Score**	**Polyphen Score**	**Exon**	**Change in amino acid**	**Global MAF (1000genome)**	**Global MAF (ESP)**
1	27	M	ERS3	Y	Y	Y	-	Y	-	-	R663C	0.02	0.99	14	c.1987C>T	0	0.000154
2	38	M	ERS3	-	-	Y	Y	-	-	-	A665T	0.57	0.002	14	c.1993G>A	0.001	N/A
3	63	M	BrS+CAD	-	Y	-	Y	Y	ICD	-	N733D	0.05	0.069	16	c.2197A>G	0	0
4	20	M	ERS3+ Bradycardia	-	Y	Y	-	Y	-	-	V734I	0.43	0.002	17	c.2200G>A	0.005	0.009236
5	20	M	ERS3+ Bradycardia	Y	Y	Y	Y	Y	ICD, Quinidine	-							
6	40	M	ERS3+AVB+ Bradycardia	Y	-	Y	Y	-	ICD	*SCN5A*							
7	20	M	ERS2 +Bradycardia	-	-	Y	-	-	-	*CACNA1C*							
8	25	M	ERS2	-	-	-	Y	-	-	*SCN10A*	V1137I	0.76	0.005	27	c.3409G>A	0.0041	0.0082
9	65	M	BrS+SQTS	Y	-	Y	Y	-	ICD	*SCN10A*, *CACNA1C*	R1197C	0.05	0.999	29	c.3589C>T	0	0
10	18	M	BrS+SAB	-	Y	Y	-	Y	-	*SCN5A*	S1402C	0	0.996	34	c.4205C>G	0	0.000077
11	39	M	BrS	Y	-	Y	Y	Y	ICD	-	L1524K fs*5	N/A	N/A	38	4570–4572 delta InsAAAT	0	0

-: No; Dx: Diagnosis; VT/VF: ventricular tachycardia/ventricular fibrillation; SCD: sudden cardiac death; MAF: the minor-allele frequency; 1000 genome: the 1000 Human Genome Project Database; ESP: exome sequencing project; ERS3: early repolarization syndrome type 3; BrS: Burgada syndrome; CAD: cardiovascular autonomic dysfunction; ICD: implantable cardioverter defibrillator; AVB: Atrioventricular Block; ERS2: ERS type 2; SQTS: short QT syndrome; SAB: Sinoatrial Block.

* FH, Family history of cardiac events/unexplained sudden death.

** Other symptoms, including palpitation, dizziness, *et al.*

Table 3

Clinical and genetic characteristics of Pedigree BS-094

Patient No.	I-1	I-2	II-1	II-2
General Information				
MMRL No.	0668	0669	0666	0667
Age	44	43	18	16
Sex	Male	Female	Male	Male
Symptom	-	-	2 syncopes	-
ICD Implanted	-	-	-	-
Electrocardiogram				
HR (bpm)	93	63(79)	71(90)	62
PR Interval (ms)	155	220(240)	190 (210)	152
QRS wave (ms)	100	90(140)	110(160)	88
QT Interval (ms)	350	480(440)	400(410)	384
QTc Interval (ms)	436	492(505)	436 (500)	390
ER pattern/J wave	+ (II, III, avF, V_6)	+ (avR, V_1, V_2)	+ (avR, V_1, V_2)	-
Ajmaline Test	N/A	+	+	N/A
Cardiac Rhythm	ERS, PVB	CCD, BrS+LQT3	BrS	-
Genotype				
SCN5A-E1784K	−/−	+/−	+/−	−/−
SUR2A-S1402C	+/−	−/−	+/−	−/−

Values in the parentheses are those after Ajmaline test.

MMRL: Masonic Medical Research Laboratory; ICD: implantable cardioverter defibrillator; HR: heart rate; bpm: beats per min; ER: early repolarization pattern; ERS: ER syndrome; PVB: premature ventricular beat; CCD: cardiac conduction disease; BrS: Brugada syndrome; LQT3: long QT type 3.